



Contents lists available at ScienceDirect



# Catalysis Today

journal homepage: [www.elsevier.com/locate/cattod](http://www.elsevier.com/locate/cattod)

## Gas phase glycerol oxidative dehydration over bifunctional V/H-zeolite catalysts with different zeolite topologies

Thamyris Q. Silva<sup>a</sup>, Maurício B. dos Santos<sup>a</sup>, Alex A.C. Santiago<sup>a</sup>, Danilo O. Santana<sup>a</sup>, Fernanda T. Cruz<sup>a</sup>, Helysa M.C. Andrade<sup>a,b</sup>, Artur J.S. Mascarenhas<sup>a,b,\*</sup>

<sup>a</sup> Laboratório de Catálise e Materiais, Departamento de Química Geral e Inorgânica, Instituto de Química, Universidade Federal da Bahia, R. Barão do Jeremoabo, s/n, Ondina, 40170-280, Salvador-Bahia, Brazil

<sup>b</sup> Instituto Nacional de Ciência e Tecnologia em Energia e Ambiente (INCT-E&A), Universidade Federal da Bahia, R. Barão do Jeremoabo, s/n, Ondina, 40170-280, Salvador, Bahia, Brazil

### ARTICLE INFO

#### Article history:

Received 10 May 2016

Received in revised form 11 July 2016

Accepted 2 August 2016

Available online xxx

#### Keywords:

Glycerol oxidative dehydration

Acrylic acid

V/H-zeolite catalysts

### ABSTRACT

The oxidative dehydration of glycerol to acrylic acid can be performed in one single step using bifunctional catalysts containing both acid and redox sites. In this sense, zeolites containing transition metals are promising catalysts. Zeolites of different topologies: FAU, FER, MEL, MFI, MOR, MWW and OFF were synthesized and further impregnated with 5% vanadium. The catalysts were characterized and evaluated in the gas phase glycerol oxidative dehydration. All catalysts showed high conversions of glycerol (100–78%). The acrolein selectivity decreases with the total density of acid sites in these zeolites. The selectivity to acrylic acid is related to the ability of each topology of stabilizing the redox pair  $V^{5+}/V^{4+}$ . The best performances were observed for zeolite catalysts with MWW, BEA and MFI topologies.

© 2016 Elsevier B.V. All rights reserved.

### 1. Introduction

The conversion of glycerol into valuable products has been investigated as a strategy to attain a sustainable biodiesel production chain [1–3]. Gas-phase glycerol dehydration to acrolein is one of the most promising route, because acrolein is an important intermediary in the production of acrylic acid, superabsorbent polymers, pharmaceuticals and plasticizers. Many acid catalysts were investigated in the literature, such as heteropolyacids, mixed oxides, phosphates and zeolites, with satisfactory glycerol conversion and acrolein selectivity [4,5]. However, rapid deactivation by coke formation is still the main limitation in their use for industrial purposes and a lot of effort has been payed to solve this problem. Among the investigated strategies, one could mention the use of moving bed reactors [6], alternating cycles of reaction and coke burning [7] or oxygen co-feeding [8]. This last option seems to be the most adequate for practical purposes, since oxidative conditions favors desorption of the oxygenate oligomer compounds that would act as coke precursors, maintaining the surface acid sites

available for further catalytic cycles of reaction and improving catalyst lifetime [9].

The acrolein, produced in a first bed containing an acid catalyst (usually a zeolite or a heteropolycompound), can be further oxidized in a consecutive bed containing a redox catalyst, such as V-W-Nb mixed oxides [10,11], resulting in high yields of acrylic acid. On the other hand, the use of catalysts containing both acid sites and redox species has been envisaged as a way to produce acrylic acid in a one-step oxy-dehydration process [1]. In most cases, it is observed an acrolein yield higher than to acrylic acid [1,12,13]. Recently, catalysts based on phosphoric acid modified W-V-Nb catalysts have shown acrylic acid yields around 60% in a short time run [14]. There is no mention to long time stability.

Redox molecular sieves, such as zeolites containing transition metal oxides, are promising alternative catalysts for this purpose, but there are few studies in the literature. Pestana et al. [1] have evaluated the zeolite-β (BEA) containing 5 wt.% or 10% of vanadium, prepared by impregnation or physical mixture, in the glycerol oxidative dehydration at 275 °C, observing a selectivity to acrylic acid of 25% and 12%, respectively, at a glycerol conversion of ca. 75%. Acrolein and acetol were the main products formed. Other oxygenates, such as acetaldehyde and acetic acid were observed as minor byproducts, but a significant amount of unidentified products with high boiling points were also formed during the reaction.

\* Corresponding author at: Laboratório de Catálise e Materiais, Departamento de Química Geral e Inorgânica, Instituto de Química, Universidade Federal da Bahia, R. Barão do Jeremoabo, s/n, Ondina, 40170-280, Salvador-Bahia, Brazil.

E-mail addresses: [ajsmascarenhas@yahoo.com.br](mailto:ajsmascarenhas@yahoo.com.br), [artur@ufba.br](mailto:artur@ufba.br)  
(A.J.S. Mascarenhas).

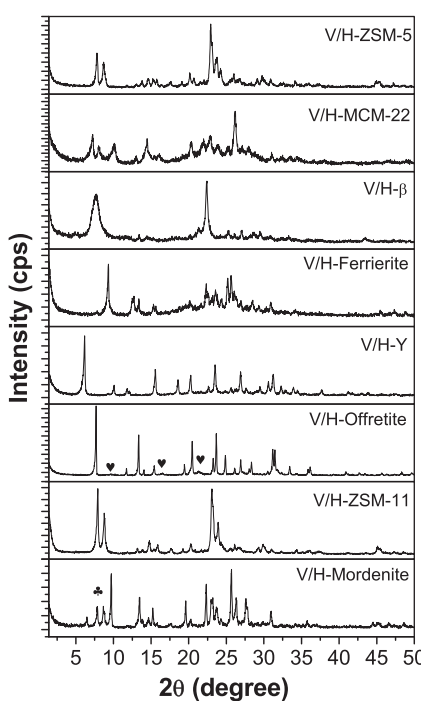


**Fig. 1.** X-ray diffraction patterns of V/H-zeolites with different topologies. (Symbols indicate the following phases: ▼, erionite zeolite and ▲, layered silicate RUB-18).

Based on XPS measurements, the authors correlated the catalytic performances to the vanadium dispersion in the zeolite pores.

In a recent publication, Possato et al. [12] have studied the use of  $V_2O_5$ /H-ZSM-5 (MFI topology) prepared by using vanadyl sulphate ( $VOSO_4$ ) or ammonium metavanadate ( $NH_4VO_3$ ) as vanadium precursors. At  $350\text{ }^\circ\text{C}$ , glycerol conversions up to 97% and selectivity to acrylic acid of 17% were attained for the catalyst prepared by wet impregnation with  $VOSO_4$  [12]. According to the authors, the presence of vanadium improved the catalyst lifetime, because catalyzes both the oxidation of acrolein to acrylic acid and the oxidation of coke precursors. The formation of acrylic acid depends on the dispersion of vanadium oxide, which facilitates the redox cycle  $V^{4+}/V^{5+}$ , as suggested by XPS and DTA analyses.

In this work, a series of catalysts were prepared by wet impregnation with 5 wt.% of vanadium using  $NH_4VO_3$  and evaluated in the gas phase oxidative dehydration of glycerol, in order to evaluate the effect of zeolite topology on the nature, dispersion and reducibility of vanadium species in the selectivity to acrylic acid.

## 2. Experimental

### 2.1. Preparation of the catalysts

Zeolite ZSM-5 (MFI), Beta (BEA), ferrierite (FER), zeolite Y (FAU), offretite (OFF) and mordenite (MOR) were synthesized according to the IZA methods [15]. The zeolite ZSM-11 (MEL) was synthesized by the method proposed by Gonzales et al. [16]. Zeolite MCM-22 (MWW) was synthesized with molar ratio  $SiO_2/Al_2O_3 = 30$  by the method proposed by Carriço et al. [7]. The calcined materials were ion exchanged with a solution with  $0.1\text{ mol L}^{-1} NH_4NO_3$  and further calcined to obtain the acid form of the respective zeolites. The thus prepared H-zeolites were wet impregnated by adding the adequate volume a solution of  $0.2\text{ mol L}^{-1}$  ammonium metavanadate ( $NH_4VO_3$ ) in order to obtain 5% of vanadium. The solvent was removed in a rotary evaporator at  $65\text{ }^\circ\text{C}$ , 30 rpm, under reduced pressure. The samples V/H-zeolite were calcined at  $500\text{ }^\circ\text{C}$ , for 3 h, under air flowing ( $50\text{ mL min}^{-1}$ ).

### 2.2. Characterization of the catalysts

The X-ray diffraction patterns (XRD) were collected on a Shimadzu XRD-6000, operating with  $CuK\alpha$  radiation at a voltage of  $40\text{ kV}$ , current of  $30\text{ mA}$ , and graphite monochromator, in the region of  $1.4^\circ$ – $80^\circ$   $2\theta$  at scan rate of  $2^\circ\text{ min}^{-1}$ .

Elemental analyses were performed by energy dispersion X-ray spectrometry in an equipment Shimadzu EDX 720, operating with rhodium radiation source at  $15\text{ kV}$  (Na-Sc) or  $50\text{ kV}$  (U-Ti) and a  $10\text{ mm}$  collimating slit.

Textural analyses were carried out by nitrogen physisorption on a Micromeritics ASAP 2020, at  $-196\text{ }^\circ\text{C}$ . The samples were pretreated at  $350\text{ }^\circ\text{C}$  for 3 h under vacuum ( $2\text{ }\mu\text{m Hg}$ ) before collecting the isotherms. BET, t-plot and BJH models were used to obtain textural properties.

Temperature programmed desorption of ammonia profiles ( $NH_3$ -TPD) were collected in a Micromeritics 2720 Chemsorb. Initially the samples were pretreated in a helium flow at  $300\text{ }^\circ\text{C}$  for 1 h.  $NH_3$  adsorption (9.9% mol/mol  $NH_3/He$ ) was carried out at ambient temperature with a flow rate of  $25\text{ mL min}^{-1}$  for 1 h. After removal of physisorbed ammonia at  $150\text{ }^\circ\text{C}$  for 1 h, the samples were heated from room temperature up to  $800\text{ }^\circ\text{C}$ , at  $10^\circ\text{ min}^{-1}$ , under helium flow ( $25\text{ mL min}^{-1}$ ). The desorbed ammonia was monitored using a thermal conductivity detector (TCD). All  $NH_3$ -TPD profiles were deconvoluted and the amounts of weak, moderate and strong acid sites were calculated.

The temperature programmed reduction profiles using  $H_2$  ( $H_2$ -TPR) were conducted in a Micromeritics 2720 Chemsorb. The samples (50 mg) were pretreated in an air flow at  $300\text{ }^\circ\text{C}$  for 1 h. After cooling down to room temperature, a flow of  $30\text{ mL min}^{-1}$  of 10 mol%  $H_2/N_2$  is admitted to the reactor, and the sample is heated from room temperature to  $1000\text{ }^\circ\text{C}$  at a heating rate  $\beta = 10\text{ }^\circ\text{C min}^{-1}$ .  $H_2$  consumption was monitored using a thermal conductivity detector.

Diffuse reflectance spectra (DRS) in the UV-vis region were collected in a Thermo-scientific Evolution 600 spectrometer operating with a Harrick Praying Mantis™ accessory in the range of  $200$ – $800\text{ cm}^{-1}$ .

Thermogravimetry (TG/DTG) of spent catalysts were conducted in a Shimadzu TGA-50 in a temperature range of  $10$ – $1000\text{ }^\circ\text{C}$  at a heating rate of  $10\text{ }^\circ\text{C min}^{-1}$  under air flow ( $50\text{ mL min}^{-1}$ ). The coke content was calculated from mass loss in the range of  $300$ – $1000\text{ }^\circ\text{C}$ .

EPR spectra of V/H-Zeolites samples were collected in tubular quartz cuvettes (width of 0.3 mm) at  $90\text{ K}$  (liquid nitrogen) with an EMX plus Bruker spectrometer using  $100\text{ kHz}$  field modulation and  $20\text{ G}$  standard modulation-width. Before the analysis, the solids samples were dried overnight at  $100\text{ }^\circ\text{C}$ .

### 2.3. Catalytic tests

The catalytic activity was evaluated in a borosilicate glass vertical fixed-bed reactor, containing  $0.1\text{ g}$  of catalyst dispersed in glass beads, operating at atmospheric pressure and  $320\text{ }^\circ\text{C}$  for 10 h. A solution of 36 wt.% glycerol in water was fed using a peristaltic pump operating at  $2\text{ mL/h}$  and an air flow of  $30\text{ mL min}^{-1}$  ( $W/F = 39.7\text{ mmol g s}^{-1}$ ). The reaction products were condensed and absorbed in  $10\text{ mL}$  of  $0.1\text{ wt\%}$  hydroquinone solution, used as polymerization inhibitor, and then analyzed by gas chromatography on a GC-FID Perkin Elmer Clarus 500 operating with a flame ionization detector using a CPWax column ( $15\text{ m} \times 0.53\text{ mm} \times 1.2\text{ }\mu\text{m}$ ). Aliquots of  $1\text{ }\mu\text{L}$  of the solution were injected. Both the injection port and detector were kept at  $250\text{ }^\circ\text{C}$ , while the following temperature program was used in the oven: i) the initial temperature was  $50\text{ }^\circ\text{C}$  for 1 min; ii) then the column was heated up to  $80\text{ }^\circ\text{C}$ , using a heating rate of  $10\text{ }^\circ\text{C min}^{-1}$ , and kept at this temperature for 3 min; and iii) finally heated up to  $220\text{ }^\circ\text{C}$ .

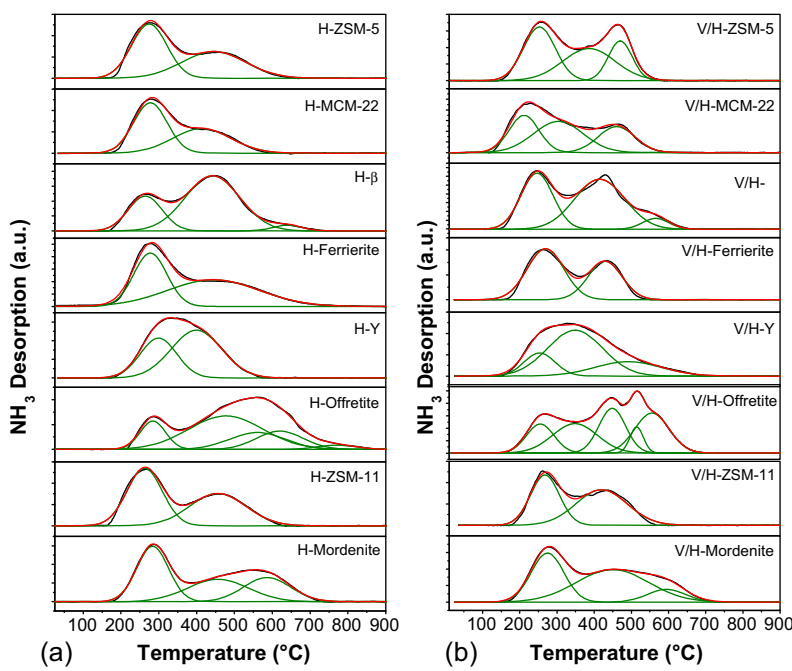


**Fig. 2.** NH<sub>3</sub>-TPD profiles of the H-zeolites of different topologies: (a) before and (b) after impregnation with 5 wt% vanadium.

at a heating rate of 12 °C min<sup>-1</sup>, and kept at this temperature for 1 min. The analysis were performed in triplicates. Pure glycerol and analytical grade reagents (possible products) were used to prepare analytical curves in the concentration range expected during the experiments, using 1-butanol as internal standard.

The glycerol conversion, product selectivities and yields were quantified according to the following equations:

$$\text{Conversion}(\%) = 100 \times (n_{\text{glycerol,in}} - n_{\text{glycerol,out}}) / n_{\text{glycerol,in}} \quad (1)$$

$$\text{Productselectivity}(\%) = 100 \times n_{\text{product,formed}} / n_{\text{glycerol,consumed}} \quad (2)$$

$$\text{Productyield}(\%) = 100 \times n_{\text{product,formed}} / n_{\text{glycerol,in}} \quad (3)$$

In which  $n_{\text{glycerol,in}}$  indicates the inlet amount of matter of glycerol;  $n_{\text{glycerol,out}}$  is the outlet amount of matter of glycerol;  $n_{\text{product,formed}}$  is the amount of matter of a given product in the effluents, and  $n_{\text{glycerol,consumed}}$  is the amount of glycerol converted during the catalytic reaction.

### 3. Results and discussion

#### 3.1. Catalyst characterization

The X-ray diffraction patterns of calcined V/H-zeolites samples with different topologies are shown in Fig. 1. The X-ray diffraction patterns confirmed the formation of a crystalline structure of the desired topologies as compared with the respective IZA standard [17]. No peaks of vanadium oxides were observed in the powder diffraction patterns, suggesting that they are very well dispersed in the pore systems of the zeolites.

The as-synthesized ferrierite presented low crystallinity, even before the impregnation with NH<sub>4</sub>VO<sub>3</sub>. The diffractograms of the samples V/H-offretite (OFF) and V/H-mordenite (MOR) suggest that these zeolites are slightly contaminated with the erionite zeolite (ERI) and the layer silicate RUB-18 phases [18], respectively.

The EDX elemental analysis of the V/H-zeolite catalysts are shown in Table 1. The experimental values of the molar ratio SiO<sub>2</sub>/Al<sub>2</sub>O<sub>3</sub> are close to those found for the materials prepared by the IZA verified synthesis methods [15]. The vanadium content is

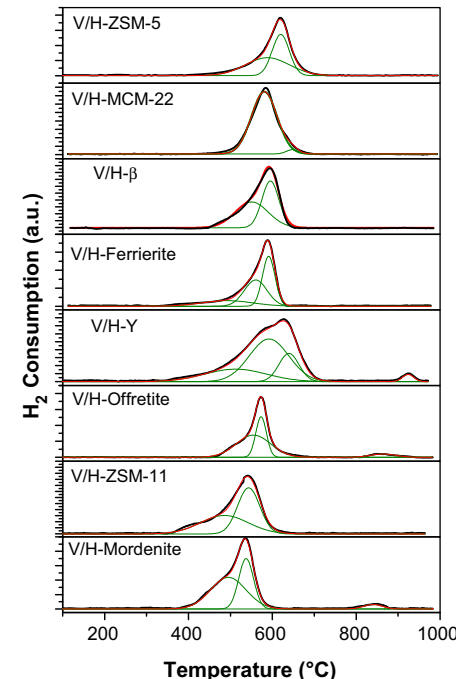


**Fig. 3.** H<sub>2</sub>-TPR profiles for the catalysts V/H-zeolites of different topologies.

close to the expected one. Differences can be accounted by the analysis error.

The acidity of the samples was studied by NH<sub>3</sub>-TPD and the profiles of the parent H-zeolites and the respective samples after impregnation with vanadium are shown in Fig. 2. Quantification of acid sites density is shown in Table 2.

The comparison of acid site strength of zeolites with different topologies by using only NH<sub>3</sub>-TPD profiles should be avoided, because different confinement events must be considered and NH<sub>3</sub> heat of protonation/adsorption does not change significantly for different zeolite topologies [19,20]. Furthermore, <sup>13</sup>C MAS NMR of

**Table 1**

Elemental analysis and textural properties for the V/H-zeolites of different topologies.

Catalyst	EDX		Textural properties – N <sub>2</sub> adsorption					
	SiO <sub>2</sub> /Al <sub>2</sub> O <sub>3</sub>		V (wt.%)	S <sub>BET</sub>	S <sub>micro</sub>	S <sub>external</sub>	V <sub>micro</sub>	V <sub>meso</sub>
	Nominal	Experimental		(m <sup>2</sup> g <sup>-1</sup> ) <sup>a</sup>	(m <sup>2</sup> g <sup>-1</sup> ) <sup>b</sup>	(m <sup>2</sup> g <sup>-1</sup> ) <sup>b</sup>	(cm <sup>3</sup> g <sup>-1</sup> ) <sup>b</sup>	(cm <sup>3</sup> g <sup>-1</sup> ) <sup>c</sup>
V/H-ZSM-5	30	20	5.1	301	209	92	0.097	0.065
V/H-MCM-22	30	22	5.4	304	214	90	0.099	0.063
V/H- $\beta$	30	25	4.2	453	368	85	0.230	0.041
V/H-Ferrierite	15.2	12	5.2	187	137	50	0.069	0.164
V/H-ZSM-11	50	42	4.8	484	362	122	0.159	0.091
V/H-Mordenite	30	14	4.6	342	296	46	0.130	0.092
V/H-Y	10	3	5.4	418	362	57	0.170	0.050
V/H-Offretite	16.5	5	4.7	364	335	29	0.156	0.008

<sup>a</sup> Surface area determined by BET method.<sup>b</sup> Micropore surface area, external surface area and micropore volume determined by t-plot method.<sup>c</sup> Average mesopore volume, determined by BJH method.**Table 2**Acid site strength distribution and quantification based on NH<sub>3</sub>-TPD profiles of V/H-zeolite catalysts.

Sample	Type of site	T <sub>m</sub> (°C)	Density of acid sites (mmol g) <sup>-1</sup>	
			Partial	Total
V/H-ZSM-5	Moderate	264	0.27	0.70
	Strong	390	0.30	(1.03) <sup>a</sup>
	Strong	477	0.13	
V/H-MCM-22	Weak	224	0.27	0.88
	Moderate	317	0.38	(0.88) <sup>a</sup>
	Strong	471	0.23	
V/H- $\beta$	Moderate	273	0.60	1.53
	Strong	423	0.83	(1.59) <sup>a</sup>
	Strong	573	0.10	
V/H-Ferrierite	Moderate	269	0.41	0.69
	Strong	429	0.28	(0.87) <sup>a</sup>
	Moderate	268	0.34	0.77
V/H-ZSM-11	Strong	420	0.43	(0.92) <sup>a</sup>
	Moderate	275	0.52	1.44
	Strong	449	0.76	(1.13) <sup>a</sup>
V/H-Mordenite	Strong	594	0.16	
	Moderate	253	0.34	2.00
	Strong	349	1.21	(2.18) <sup>a</sup>
V/H-Y	Strong	491	0.45	
	Moderate	266	0.33	2.06
	Strong	358	0.55	(2.10) <sup>a</sup>
	Strong	456	0.50	
	Strong	520	0.15	
V/H-Offretite	Strong	561	0.57	
	Moderate			
	Strong			
	Strong			
	Strong			

<sup>a</sup> Values in parenthesis indicates the total density of acid sites before impregnation of the H-zeolite with vanadium.

adsorbed acetone has detected no differences in acid strength in high silica zeolites [21]. However, in this work, only a comparison for the same zeolite topology, before and after impregnation with 5 wt.% of vanadium, has been performed.

All materials have shown high acid sites densities (Table 2). From the NH<sub>3</sub>-TPD profiles of Fig. 2a, one could observe that zeolites H-ZSM-5, H-MCM-22, H-Ferrierite, H-Y and H-ZSM-11 have presented two events of NH<sub>3</sub> desorption, suggesting the presence of at least two types of sites with different acid strength. Besides, zeolites H- $\beta$  and H-mordenite showed three events, while four desorption events are seen for zeolite H-offretite. For these last materials, it is important to consider the presence of contaminant phases of other zeolite topologies and/or layered silicates detected by XRD.

The values of acid sites density for the H-zeolite samples correlate well with their respective molar ratio SiO<sub>2</sub>/Al<sub>2</sub>O<sub>3</sub>, differences being accounted by the material crystallinity and the presence of defects. In general, the addition of vanadium leads to a decrease in the acidity with respect to the parent H-zeolites (Table 2), but also creates new acid sites, probably of Lewis type.

Fig. 3 shows the profiles of H<sub>2</sub>-TPR for the catalysts V/H-zeolite with different topologies. One could observe a large reduction peak between 300 and 700 °C, due to the reduction of vanadium oxide species. This peak can be shifted to lower or to higher temperatures depending on the dispersion and location of vanadium species in the porous systems (channels and/or cavities) of the different zeolite topologies [21]. The high temperature peak ( $T_m > 800$  °C) corresponds to the non-stoichiometric reduction  $V^{+5} \rightarrow V^{+3.32}$  [22].

A tentative assignment of the reduction peaks can be performed by quantifying the molar ratio H<sub>2</sub>/V. The nominal values for the reduction  $V^{4+} \rightarrow V^{3+}$  and  $V^{5+} \rightarrow V^{3+}$  are 0.5 and 1.0, respectively [23]. For all samples the molar ratio H<sub>2</sub>/V is between these nominal values, as shown in Table 3, what suggests that vanadium exists in both oxidation states, V<sup>5+</sup> and V<sup>4+</sup> in different proportions, in the fresh catalysts. For the material V/H-Y the molar ratio H<sub>2</sub>/V is 0.91, which indicates that vanadium is better stabilized as V<sup>5+</sup> in FAU topology. The zeolites with topologies MWW and BEA have shown molar ratios H<sub>2</sub>/V close to 0.5, but it is unacceptable that all vanadium atoms present in these catalysts would be in the V<sup>4+</sup> oxidation

**Table 3**

$H_2$ -TPR quantitative analyses of V/H-zeolite with different topologies, indicating onset and maximum reduction temperature, and molar ratio  $H_2/V$ .

Sample	$T_0$ (°C)	$T_{M1}$ (°C)	$T_{M2}$ (°C)	$T_{M3}$ (°C)	$H_2/V$
V/H-ZSM-5	430	588	620	–	0.60
V/H-MCM-22	388	540	586	–	0.47
V/H- $\beta$	380	506	555	–	0.54
V/H-Ferrierite	269	514	550	–	0.61
V/H-Y	389	582	627	924	0.91
V/H-Offretite	463	500	575	857	0.38
V/H-ZSM-11	352	396	545	–	0.69
V/H-Mordenite	374	467	538	–	0.44

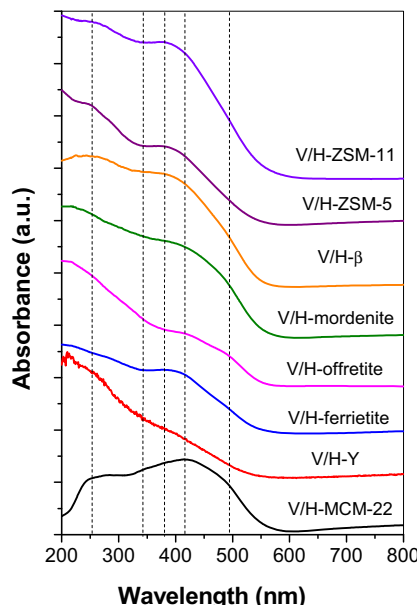


**Fig. 4.** Diffuse reflectance UV-vis spectra recorded at room temperature of V/H-zeolite of different topologies. Spectra were measured using the respective H-zeolite as reference.

state, because the materials have the characteristic yellow-brown color of  $V_2O_5$ . As the molar ratio  $H_2/V$  nominal for  $V^{5+}$  to  $V^{4+}$  reduction is also 0.5, it would be more reasonable to assume that  $V^{5+}$  in the V/H-MCM-22 and V/H- $\beta$  materials do not reduce until  $V^{3+}$  and that the redox cycle  $V^{5+}/V^{4+}$  would be favored in these topologies. Finally yet importantly, the molar ratio  $H_2/V$  for V/H-offretite and V/H-mordenite samples is lower than 0.5, which suggests the formation of non-stoichiometric species of vanadium oxide [23], what can also occur for other materials.

The nature and chemical environment of the vanadium species were also studied by diffuse reflectance spectroscopy in the UV/vis region (Fig. 4). In the spectra of Fig. 4, it is possible to observe bands at 270 and 340 nm, that can be assigned to  $\pi(t_2) \rightarrow d(e)$  and to  $\pi(t_1) \rightarrow d(e)$  charge transfer transitions of tetrahedral  $V^{5+}$  [24]. A band at 380 nm reveal the presence of  $V^{5+}$  ions in oxide clusters dispersed in the porous systems of the zeolites. Hydrated species, like octahedral vanadium ions contribute to the absorption in the 300–500 nm region and, finally a wide band from 500 to 800 nm is typical of d-d transitions of  $V^{4+}$  [25,26]. Except for V/H-Y, all samples present a contribution above 500 nm, confirming that  $V^{4+}$  ions are present in these zeolite topologies. These results reinforce the attribution of the  $H_2$ -TPR reduction peaks herein proposed.

In order to obtain more information about the nature and coordination of the V-oxide species present within the zeolite framework by monitoring the  $V^{4+}$  species, the samples were analyzed by EPR at 90 K. It is important to remember that  $V^{5+}$  ( $d^0$ ) is silent in the electron paramagnetic resonance spectroscopy. The EPR spectra of all samples confirmed the presence of significant

amount of  $V^{4+}$  ions (Fig. 5). Vanadium(IV) has an electronic configuration  $d^1$ , with net electron spin ( $S = 1/2$ ) and net nuclear spin ( $I = 7/2$ ), thus each signal originates  $2I + 1 = 2 \times 7/2 + 1 = 8$  lines due to hyperfine interactions [27].

The analysis of the spectra shown in Fig. 5a–h revealed that, even without a reduction pretreatment, all samples have presented a signal with  $g_{\parallel} = 1.936$  and  $A_{\parallel} = 203$  G,  $g_{\perp} = 1.990$  and  $A_{\perp} = 83$  G. These tensor values are consistent with the presence of  $VO^{2+}$  ions in an axially symmetric environment, probably with  $V^{4+}$  in a distorted octahedral geometry or square pyramidal coordination, typical of hydrated  $VO^{2+}$  ions in cation exchange sites [28,29].

Observing the EPR spectra, one could relate the normalized intensities with the content of  $V^{4+}$  species in each sample, and the following order is observed: V/H- $\beta$  > V/H-MCM-22 > V/H-offretite > V/H-ZSM-11 > V/H-mordenite > V/H-ZSM-5 ~ V/H-ferrierite ~ V/H-Y, which is consistent to the previously discussed based on TPR analysis.

### 3.2. Catalytic tests

Fig. 6 shows the conversion of glycerol and the selectivity to products as a function of reaction time in the oxidative dehydration of glycerol.

The glycerol conversion for all catalysts was high during the 10 h reaction runs and the main reaction product is acrolein, and not acrylic acid, regardless of the catalyst employed. Comparing the results with those previously reported in the absence of oxygen [7,9], deactivation by coke deposition is highly inhibited in the presence of oxygen and a decrease of ca. 20% in glycerol conversion was observed for V/H-MCM-22 and V/H-ZSM-11 catalysts, while V/H-ZSM-5 and V/H-mordenite were more stable during the 10 h of reaction.

The catalyst V/H-ZSM-11 has presented higher selectivity to acrolein in the first hours, but V/H-MCM-22 was more stable in terms of selectivity to acrolein. The following order was observed for the selectivity to acrolein after 10 h of reaction: V/H-MCM-22 > V/H-ZSM-11 ~ V/H-ZSM-5 ~ V/H- $\beta$  ~ V/H-ferrierite > V/H-mordenite > V/H-Y > V/H-offretite.

The selectivity to acrylic acid is very low in the first hour, but increases with the reaction time, indicating that re-adsorption of acrolein on vanadium oxides species is limiting the oxidation step. After 10 h on stream, catalysts V/H-MCM-22 and V/H- $\beta$  reach 20% of selectivity to acrylic acid. The results obtained with the catalyst 5% V/H-Beta are similar to those reported by Pestana et al. [1] for the same type of catalyst, even if operating at higher temperature. Besides, the catalytic performances obtained here with the catalyst V/H-ZSM-5 is superior to those reported by Possato et al. [12] with a similar catalyst.

The product distribution in the oxidative dehydration of glycerol for the V/H-zeolites with different topologies is shown in Table 4 for the condensates obtained after 2 and 10 h of reaction, respectively. Even though acrolein was the main product, significant amounts of acrylic acid, acetic acid and acetaldehyde were also formed. Coke

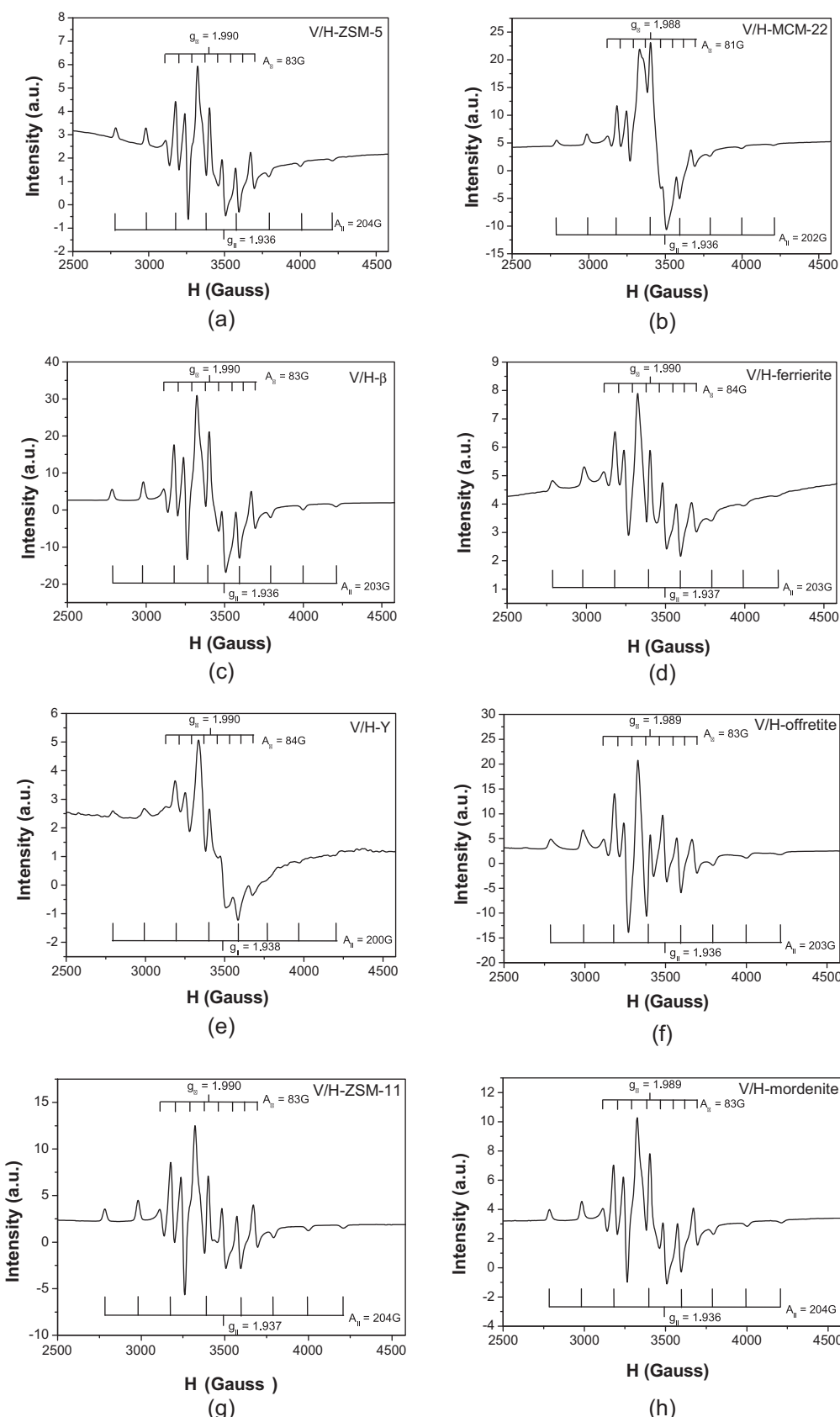


**Fig. 5.** EPR spectra recorded at 90 K of calcined V/H-Zeolite with different topologies.

**Table 4**

Catalytic performance for the gas-phase oxydehydration of glycerol over V/H-zeolites with different topologies, after 2 h and 10 h.

Catalyst	MFI	MWW	BEA	FER	FAU	OFF	MEL	MOR
Conversion (%) <sup>a</sup>	99.4 (95.9)	95.3 (76.2)	93.8 (87.6)	90.7 (81.7)	91.1 (81.3)	97.1 (84.2)	99.9 (80.3)	98.0 (89.7)
Acrolein yield (%) <sup>a</sup>	53.8 (46.8)	64.1 (42.8)	52.8 (40.5)	52.1 (37.7)	30.8 (23.2)	24.2 (12.7)	75.6 (40.9)	46.8 (32.1)
Acrylic Acid yield (%)	3.2 (12.0)	10.4 (16.0)	6.1 (17.7)	2.9 (5.5)	0.5 (1.1)	0.7 (1.8)	1.7 (11.6)	0.6 (3.2)
<i>Molar selectivity (%)</i>								
Acrolein	54.2 (48.7)	67.3 (56.6)	56.4 (46.3)	57.4 (46.4)	33.8 (28.6)	24.9 (15.1)	75.7 (50.9)	47.8 (35.8)
1-hydroxyacetone	0.1 (0.1)	0.3 (0.3)	0.4 (0.2)	0.6 (0.9)	0.3 (0.3)	0.2 (0.3)	0.0 (0.3)	0.1 (0.4)
Propionaldehyde	2.1 (2.3)	3.7 (3.1)	4.2 (1.6)	4.4 (4.8)	0.5 (0.5)	0.3 (0.3)	0.9 (0.3)	0.4 (0.5)
Acetaldehyde	3.0 (3.8)	6.5 (5.5)	8.3 (5.6)	10.6 (13.5)	7.6 (8.0)	2.8 (5.8)	14.6 (4.0)	7.6 (15.5)
Acetic acid	1.4 (2.0)	1.1 (4.1)	5.2 (6.0)	5.4 (12.1)	1.7 (4.8)	6.2 (7.1)	5.3 (2.9)	1.8 (7.3)
Allyl Alcohol	0.0 (0.2)	0.6 (0.6)	1.6 (0.4)	3.5 (4.1)	0.3 (0.5)	0.2 (0.4)	0.0 (0.1)	0.2 (0.8)
Propionic acid	0.0 (0.0)	0.9 (1.4)	2.4 (2.2)	0.9 (1.1)	0.4 (1.1)	0.5 (2.3)	1.1 (2.0)	1.8 (0.7)
Acrylic acid	3.2 (12.5)	10.9 (21.0)	6.5 (20.2)	2.4 (6.7)	0.5 (1.3)	0.7 (2.1)	1.7 (14.5)	0.6 (3.6)
Others	36.0 (30.5)	8.7 (7.8)	15.0 (17.7)	14.2 (10.4)	54.9 (55.0)	64.2 (66.6)	0.8 (25.0)	40.3 (35.5)
Coke (%) <sup>c</sup>	7.5	10.3	12.7	5.0	7.2	4.1	6.7	6.8

<sup>a</sup> Reaction conditions: 320 °C, 36.6% glycerol; glycerol flow = 2 mL/h, catalyst weight = 0.10 g.

**Table 5**

Comparison of V/H-zeolite catalyst performances in the gas-phase glycerol oxidehydration, after 10 h of run, with data reported in the literature.

Catalyst	WHSV (h <sup>-1</sup> )	T (°C)	c <sub>glycerol</sub> (%)	S <sub>acrolein</sub> (%)	S <sub>acrylic acid</sub> (%)	Reference
Zeolitic	V/H-MCM-22	8.6	320	76.2	56.2	21
	V/H-b	8.6	320	87.6	46.3	20.2
	V/H-ZSM-5	8.6	320	95.9	48.7	12.5
	V/H-ZSM-11	8.6	320	80.3	50.9	14.5
	V <sub>2</sub> O <sub>5</sub> -ZSM-5	3.07	350	97	15	[12]
	5%V-BEA	1.51	275	75	45	[1]
	Fe <sub>4.0</sub> -BEA-50	7.56	275	100	13	[38]
Non zeolitic	MoV/SiW/Al <sub>2</sub> O <sub>3</sub>	0.31	300	100	2.9	12.1
	SiW/Al <sub>2</sub> O <sub>3</sub> and Mo <sub>3</sub> VO <sub>x</sub>	0.31	350	100	35.2	19.8
	SiW/Al <sub>2</sub> O <sub>3</sub> and Mo <sub>3</sub> VO <sub>x</sub>	0.31	450	100	3	46.2
	SiW/Al <sub>2</sub> O <sub>3</sub> and Mo <sub>3</sub> VO <sub>x</sub> (phy.mix.)	0.31	450	100	0.9	[30]
	V-W-Nb-oxides	1.24	290	100	17	34
	V-W-oxides	1.21	300	90	20	[31]
	V-Mo-oxides	0.11	300	90	10	[32]
	Mo-V-W-oxides	0.42	250	100	8.2	30.5
	V-W-oxides	0.6	300	100	0.1	[34]
	V-W-oxides	0.6	300	100	3	[34]
	V-Mo-Te-Nb-oxides	0.6	300	99	2	[34]
	V-W-oxides	1.41	310	100	11	[35]
	V-W-Nb-oxides	1.93	265	100	3	[36]
	Cs(VO) <sub>0.2</sub> (PMo) <sub>0.5</sub> (PW) <sub>0.5</sub>	0.5	340	100	6.9	[37]
	1Cs(VO) <sub>0.2</sub> PMoW	0.5	340	100	9.3	40.9
	H <sub>0.1</sub> Cs <sub>2.5</sub> (VO) <sub>0.2</sub> (PMo <sub>12</sub> O <sub>40</sub> ) <sub>0.25</sub> (PW <sub>12</sub> O <sub>40</sub> ) <sub>0.75</sub>	0.5	340	100	18	[37]

contents determined by TG analysis under oxidative conditions after 10 h of catalytic run were also shown in Table 4.

In order to establish structure-activity relationships for the glycerol oxidative dehydration, acrolein and acrylic acid yields were plotted as a function of acid sites density and molar ratio V<sup>5+</sup>/V<sup>4+</sup> (determined by H<sub>2</sub>-TPR), respectively. The results are shown in Fig. 7a and b.

In general, Fig. 7a suggests that acrolein yield tends to decrease with the increase of acid sites density. Probably this is a consequence of deactivation by coke (see Table 4) and/or non-condensable products (gases), which were not quantified. The best results were observed for the catalysts whose acid sites density was near to 0.8 mmol g<sup>-1</sup>, however among these catalysts it was noticeable the influence of the zeolite topology, with V/H-ZSM-11 (MEL)>V/H-MCM-22 (MWW)>V/H-ZSM-5 (MFI)~V/H-ferrierite (FER).

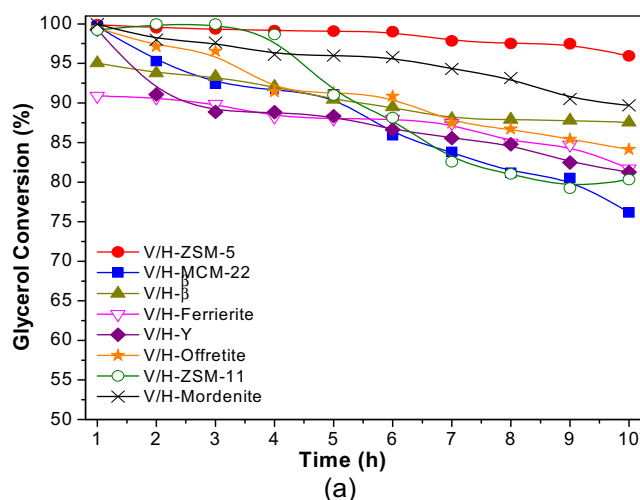
On the other hand, for acrylic acid (Fig. 7b), one can observe that those catalysts presenting a molar ratio V<sup>5+</sup>/V<sup>4+</sup> around 0.5 have shown higher yields, confirming that the stabilization of the redox pair V<sup>5+</sup>/V<sup>4+</sup> favors the catalytic cycle and suggests that the reaction occurs according to the Mars-van Krevelen mechanism [30], as follows:

- i) glycerol interacts via C<sub>2</sub>-hydroxyl group with zeolite Brønsted acid sites, producing by dehydration 3-hydroxipropionaldehyde as an intermediary, which is further dehydrated to produce acrolein [31];
- ii) acrolein re-adsorbs on vanadium species and is oxidized to acrylic acid, with consequent reduction of V<sup>5+</sup> to V<sup>4+</sup>, which stabilizes the oxygenated species as acrylate [32];
- iii) V<sup>4+</sup> ions are re-oxidized to V<sup>5+</sup> by consuming molecular oxygen in the process.

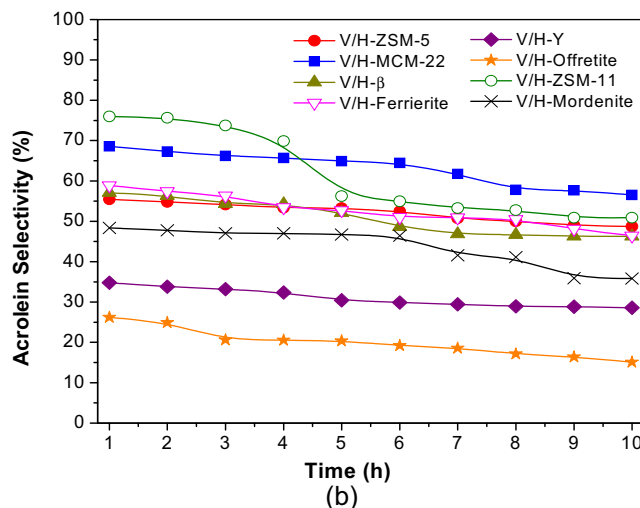
### 3.3. Comparison with literature

The bifunctional V/H-zeolites catalysts of different zeolite topologies were compared those found in the literature. Table 5 shows not only glycerol conversion and selectivities to acrolein and acrylic acid, but also the reaction conditions as temperature and weight hourly space velocity (WHSV = mass flow/catalyst mass).

For catalysts in the literature, acid function is provided by a zeolite [1,12,33], a heteropolyacids [30] or an acid support, such as alumina [34] or niobia [8,10,35], while transition metal oxides, as vanadium, molybdenum or tungsten, or their associations provide the catalyst redox function [8,10,32,34,36,37]. MoVW catalyst, containing niobium or not in their formulation, are the most promising



(a)



(b)

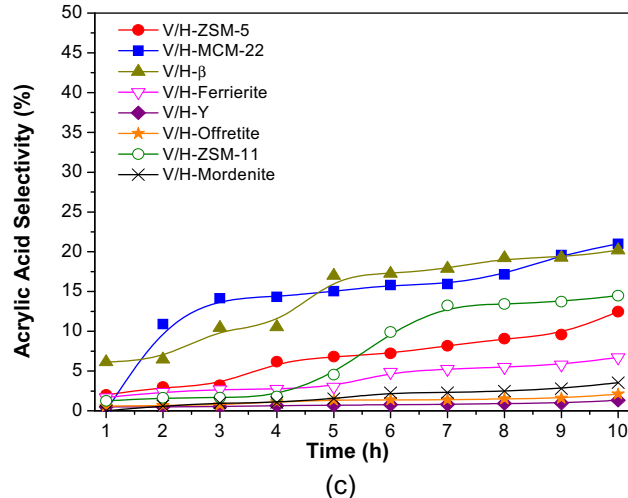
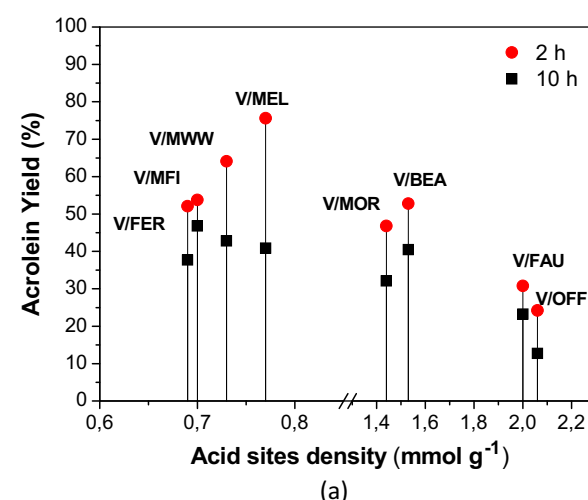


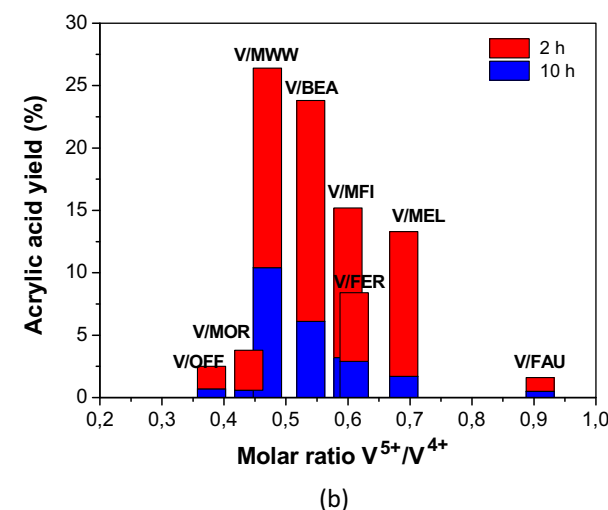
**Fig. 6.** Glycerol conversion (a), acrolein selectivity (b) and acrylic acid selectivity over V/H-Zeolite catalysts. Reaction conditions: 320 °C, 36.6% glycerol; glycerol flow = 2 mL/h, catalyst weight = 0.10 g.

catalysts, with higher acrylic acid selectivities than those based on zeolites. However, it is necessary to consider that they operate with low space velocities, which means that space time (W/F) is high, facilitating acrolein re-adsorption on vanadium species (step ii).

Bifunctional V/H-MCM-22 (MWW topology) reached maximum 21% of acrylic acid selectivity under WHSV = 8.6 h<sup>-1</sup> and temper-



(a)



(b)

**Fig. 7.** Structure-activity relationships: (a) dependence of acrolein yield (after 2 h and 10 h) on the acid sites density; and (b) acrylic acid yield (after 2 h and 10 h) as a function of the molar ratio V<sup>5+</sup>/V<sup>4+</sup>. Reaction conditions: 320 °C, 36.6% glycerol; glycerol flow = 2 mL/h, catalyst weight = 0.10 g.

atures of 320 °C, suggesting that the catalytic performance can be improved by adjusting the hydrodynamic properties of the catalytic reactor. Additionally, as the oxygen content is crucial to the regeneration of redox sites, catalytic performance should be improved by increasing molar ratio O<sub>2</sub>/glycerol.

#### 4. Conclusions

Bifunctional catalysts V/H-zeolite, prepared by impregnation of V<sub>2</sub>O<sub>5</sub> on the acid zeolites of different topologies, have shown to be very active in the gas-phase oxidative dehydration of glycerol, achieving high glycerol conversions and producing mainly acrolein and acrylic acid. Among these catalysts, those with MWW and BEA topologies resulted in better catalytic performances, with selectivities to acrylic acid of about 20%, but a significant coke deposition was observed for these more open topologies. Characterization techniques suggested that acrolein production is favored on catalysts in which acid sites densities are around 0.8 mmol g<sup>-1</sup>, but the effect of zeolite topology must be considered. On the other hand, acrylic acid selectivities are related to the ability of a specific zeolite topology to stabilize the redox pair V<sup>5+</sup>/V<sup>4+</sup>, as evidenced by H<sub>2</sub>-TPR, DRS UV-vis and EPR, suggesting that a Mars van Krevelen mechanism is occurring. These catalysts are promising for practi-

cal uses, but reaction parameters as space velocity and molar ratio oxygen/glycerol must be optimized.

## Acknowledgments

T. Q. Silva thanks to National Council of Technological and Scientific Development (CNPq) and Institutional Programme of Scientific Initiation (PIBIC/UFBA) for the scholarship.

## References

- [1] C.F.M. Pestana, A.C.O. Guerra, G.B. Ferreira, C.C. Turci, C.J.A. Mota, J. Braz. Chem. Soc. 24 (2013) 100–105.
- [2] M. Pagliaro, R. Ciriminna, H. Kimura, M. Rossi, C.D. Pina, Angew. Chem. Int. 46 (2007) 4434–4440.
- [3] S. Bagheri, N.M. Julkapli, W.A. Yehye, Renew. Sust. Energy Rev. 41 (2015) 113–127.
- [4] A. Talebian-Kiakalaieh, N.A. SaidinaAmin, H. Hezaveh, Renew. Sust. Energy Rev. 40 (2014) 28–59.
- [5] B. Katryniok, S. Paul, F. Dumeignil, ACS Catal. 3 (2013) 1819–1834.
- [6] A. Corma, G.W. Huber, L. Sauvanaud, P. O'Connor, J. Catal. 257 (2008) 163–171.
- [7] C.S. Carriço, F.T. Cruz, M.B. Santos, H.O. Pastore, H.M.C. Andrade, A.J.S. Mascarenhas, Micropor. Mesopor. Mater. 181 (2013) 74–82.
- [8] J. Deleplanque, J.-L. Dubois, J.-F. Devaux, W. Ueda, Catal. Today 157 (2010) 351–358.
- [9] M.B. dos Santos, H.M.C. Andrade, A.J.S. Mascarenhas, Micropor. Mesopor. Mater. 223 (2016) 105–113.
- [10] A. Chieregato, F. Basile, P. Concepción, S. Guidetti, G. Liosi, M.D. Soriano, C. Trevisanut, F. Cavani, J.M.L. Nieto, Catal. Today 197 (2012) 58–65.
- [11] R. Liu, T. Wang, D. Cai, Y. Jin, Ind. Eng. Chem. Res. 53 (2014) 8667–8674.
- [12] L.G. Possato, W.H. Cassinelli, T. Garetto, S.H. Pulcinelli, C.V. Santilli, L. Martins, Appl. Catal. A 492 (2015) 243–251.
- [13] M. Massa, A. Andersson, E. Finocchio, G. Busca, F. Lenrick, L.R. Wallenberg, J. Catal. 297 (2013) 93–109.
- [14] K. Omata, K. Matsumoto, T. Murayama, W. Ueda, Catal. Today 259 (2015) 205–212.
- [15] Verified Syntheses of Zeolitic Materials, in: H. Robson (Ed.), 2nd ed., Elsevier, Amsterdam, 2001.
- [16] G.G. Gonzalez, M.E. Gomes, G. Vitale, G.R. Castro, Micropor. Mesopor. Mater. 121 (2009) 26–33.
- [17] M.M.J. Treacy, J.B. Higgins, Collection of Simulated XRD Power Patterns for Zeolites, 4th ed., Elsevier, Amsterdam, 2001.
- [18] F.S.O. Ramos, H.O. Pastore, Micropor. Mesopor. Mater. 177 (2013) 143–150.
- [19] E.G. Derouane, C.D. Chang, Micropor. Mesopor. Mater. 35 (2000) 425–433.
- [20] M. Brandle, J. Sauer, J. Am. Soc. 120 (1998) 1556–1570.
- [21] A. Biaglow, R.J. Gorte, D. White, J. Catal. 150 (1994) 221–224.
- [22] W. Li, L. Luo, H. Yamashita, J.A. Labinger, M.E. Davis, Micropor. Mesopor. Mater. 37 (2000) 57–65.
- [23] F. Arena, F. Frusteri, A. Parmaliana, Appl. Catal. A 176 (1999) 189–199.
- [24] A.E. Lewandowska, M.A. Baranowska, F. Tielen, M. Che, S. Dzwigaj, J. Phys. Chem. C 114 (2010) 19771–19776.
- [25] A. Albuquerque, H.O. Pastore, L. Marchese, Stud. Surf. Sci. Catal. 158 (2005) 901–908.
- [26] S. Dzwigaj, E. Ivanova, R. Kefirov, K. Hadjivanov, F. Averseng, J.M. Krafft, M. Che, Catal. Today 142 (2009) 185–191.
- [27] K. Dyrek, M. Che, Chem. Rev. 97 (1997) 305.
- [28] E.-M. El-Malki, P. Massiani, M. Che, Res. Chem. Intermed. 33 (2007) 749–774.
- [29] R. Baran, Y. Millot, T. Onfray, F. Averseng, J.-M. Krafft, S. Dzwigaj, Micropor. Mesopor. Mater. 161 (2012) 179–186.
- [30] X. Li, Y. Zhang, ACS Catal. 6 (2016) 2785–2791.
- [31] E. Yoda, A. Ootawa, Appl. Catal. A 360 (2009) 66–70.
- [32] Y.S. Yun, K.R. Lee, H. Park, T.Y. Kim, D. Yun, J.W. Han, J. Yi, ACS Catal. 5 (2015) 82–94.
- [33] M.M. Diallo, J. Mijoin, S. Laforgue, Y. Pouilloux, Catal. Commun. 79 (2016) 58–62.
- [34] L. Liu, B. Wang, Y. Du, Z. Zhong, A. Borgna, Appl. Catal. B. Environ. 174–175 (2015) 1–12.
- [35] A. Chieregato, M.D. Soriano, F. Basile, G. Liosi, S. Zamora, P. Concepción, F. Cavani, J.M. López Nieto, Appl. Catal. B Environ. 150–151 (2014) 37–46.
- [36] L. Shen, H. Yin, A. Wang, X. Lu, C. Zhang, Chem. Eng. J. 244 (2014) 168–177.
- [37] M.D. Soriano, P. Concepción, J.M. López Nieto, F. Cavani, S. Guidetti, C. Trevisanut, Green Chem. 13 (2011) 2954–2962.